Biochemical and biophysical comparison of human and mouse beta-2 microglobulin reveals the molecular determinants of low amyloid propensity

Adnane Achour[1#], Luca Broggini[2], Xiao Han[1], Renhua Sun[1], Carlo Santambrogio[3], Jeremie Buratto[1], Cristina Visentin[2], Alberto Barbiroli[4], Chiara Maria Giulia De Luca[5], Pietro Sormanni[6], Fabio Moda[5], Alfonso De Simone[7], Tatyana Sandalova[1], Rita Grandori[3], Carlo Camilloni[2#], Stefano Ricagno[2#]

[1]Science for Life Laboratory, Department of Medicine Solna, Karolinska Institute, and Division of Infectious Diseases, Karolinska University Hospital, Solna, SE-17176 Stockholm, Sweden;
[2]Dipartimento di Bioscienze, Università degli Studi di Milano, Milan, Italy;
[3]Dipartimento di Biotecnologie e Bioscienze, Università Milano-Bicocca, Milan, Italy;
[4]Dipartimento di Scienze per gli Alimenti, la Nutrizione e l′Ambiente, Università degli Studi di Milano, Milan, Italy;
[5]Fondazione IRCCS Istituto Neurologico Carlo Besta, Divisione di Neurologia 5 - Neuropatologia, 20133 Milano, Italy;
[6]Department of Chemistry, University of Cambridge, CB2 1EW, UK;
[7] Department of Life Sciences, Imperial College London, South Kensington, SW7 2AZ, UK.

Correspondence: Adnane Achour, Science for Life Laboratory, Department of Medicine Solna, Karolinska Institute, and Division of Infectious Diseases, Karolinska University Hospital, Stockholm, Sweden, Tel: (+46) 703951023 E-mail: adnane.achour@ki.se; Carlo Camilloni, Dipartimento di Bioscienze, Università degli Studi di Milano, Milan, Italy, Tel: (+39) 02 50314918, E-mail: carlo.camilloni@unimi.it; Stefano Ricagno, Dipartimento di Bioscienze, Università degli Studi di Milano, Milan, Italy, Tel: (+39) 02 50314914, E-mail: stefano.ricagno@unimi.it.

Running title: Murine beta-2 microglobulin amyloid propensity

Article type   : Original Article

ABSTRACT
The molecular bases of amyloid aggregation propensity are still poorly understood, especially for proteins that display a stable folded native structure. A prototypic example is human beta-2 microglobulin (β2m), which, when accumulated in patients, gives rise to dialysis-related amyloidosis. Interestingly, although the physiologic concentration of β2m in mice is five times higher than that found in human patients, no amyloid deposits are observed in mice. Moreover, murine β2m not only displays a lower amyloid propensity both *in vivo* and *in vitro*, but also inhibits the aggregation of human β2m *in vitro*. Here we compared human and murine β2m for their aggregation propensity, ability to form soluble oligomers, stability, three-dimensional structure and dynamics. Our results indicate that murine β2m low-aggregation propensity is due to two concomitant aspects: the low aggregation propensity of its primary sequence combined with the absence of high-energy amyloid-competent conformations under native conditions. The identification of the specific properties

determining the low aggregation propensity of mouse β2m will help delineate the molecular risk factors which cause a folded protein to aggregate.

INTRODUCTION

The 99-residue-long β2m protein is the invariable subunit, non-covalently bound to the heavy chain in major histocompatibility complex class I molecules (MHC-I). The globular β2m molecule displays a typical immunoglobulin-like fold with seven β-strands arranged in two β-sheets, ABDE and CFG, linked by a disulphide bond [1]. The overall stability of MHC-I/peptide complexes depends on the qualities and affinity of the bound antigen [2-5]. When β2m interacts with the MHC-I heavy chain, it is highly stabilised while the unbound β2m monomer may exert its amyloidogenic potential [6]. Indeed, it is well established that human β2m (hβ2m) is an aggregation-prone protein responsible for at least two types of amyloid-related diseases. The aggregation of wild type hβ2m induces Dialysis-Related Amyloidosis (DRA) [7]. Conversely, a severe hereditary systemic amyloidosis is linked to the D76N variant of hβ2m [8]. Physiologically, hβ2m is degraded in the kidneys. Thus, DRA patients typically suffer from kidney dysfunction with a consequent accumulation of hβ2m. Over the years, such pathologically high concentration results in aggregation and amyloid deposition in the skeletal joints, bones and muscles, leading to bone fragility and movement impairment [9]. Interestingly, while a hβ2m concentration up to 4.3 µM is typical for DRA patients [10], the physiologic concentration of murine β2m (mβ2m) is usually around 22 µM but no amyloid aggregation is observed in the mouse [11]. This indicates a much lower amyloidogenic potential for mβ2m compared to hβ2m. The picture is however more complex as Zhang *et al* showed that overexpressed hβ2m in mouse does not aggregate, suggesting that either some molecular elements necessary to aggregation are missing or that the mouse life span is not sufficient for hβ2m to successfully aggregate [12]. *In vitro*, Pashley *et al.* identified the increased solubility of mβ2m as the main reason for its lower aggregation propensity compared to hβ2m [13]. Intriguingly, Radford and co-workers recently demonstrated that despite both hβ2m and its highly aggregation-prone truncated variant ΔN6-hβ2m can interact with mβ2m, mβ2m does not aggregate. Moreover, the murine protein is capable to inhibit the aggregation of both hβ2m and ΔN6-hβ2m [14, 15].

Altogether, a solid amount of previous work has demonstrated that hβ2m aggregation propensity stems from several specific properties, including the stability of the folded state [14, 16, 17] as well as the presence of several aggregation prone residues on the surface of hβ2m [18, 19]. Recent publications have also highlighted the crucial role of protein dynamics in determining hβ2m aggregation propensity by exposing aggregation prone regions [18, 20].

In order to shed further light into how mβ2m is protected from amyloid aggregation and can unexpectedly act as an inhibitor of hβ2m amyloid formation, a mixed structural, biophysical and computational approach was undertaken.

RESULTS

mβ2m displays lower amyloid propensity compared to hβ2m

It has been previously demonstrated that mβ2m does not display the aggregation propensity typical of hβ2m [11, 13]. We initiated the present study by testing two different well-established aggregation protocols to confirm these observations. Soluble hβ2m and mβ2m were incubated 100 hours at 37 °C at pH 2.5 and at pH 7.4 in presence of 20% v/v 2,2,2 trifluoroethanol (TFE). Incubations were performed both in absence and presence of seeds prepared from preformed hβ2m fibrils [21]. Our results confirm that hβ2m aggregates abundantly under both these conditions, while mβ2m remains soluble and does not display any sign of aggregation (Fig. 1A-B). A sequence-based analysis of the solubility – and in turn aggregation propensity - of mβ2m or hβ2m using CamSol [22] revealed that the overall aggregation propensity is comparable along the two protein sequences except for the regions corresponding to amino acid residues 60-70 (E strand) and 80-90 (F-G strands). Our analysis

indicated that these two regions are markedly more aggregation prone in hβ2m than in mβ2m (Fig. 1C).

Under native conditions mβ2m forms less oligomers compared to hβ2m

Native mass-spectrometry (MS) was thereafter employed to assess the oligomerization propensity of hβ2m and mβ2m under non-denaturing conditions. As previously shown, hβ2m displays a pronounced tendency to oligomerize under native conditions [23], with a considerable protein fraction (~20%) in oligomeric states of variable stoichiometry (dimer and trimer) (Fig. 2A). Under the same experimental conditions, mβ2m displays a significantly reduced propensity to form oligomers, with only a minor fraction of the population (~2%) detectable in the dimeric state and no higher-order species (Fig. 2B). This reduced oligomerization tendency under native-like conditions could be related to the lower aggregation propensity of mβ2m relative to hβ2m. The murine D85V variant (see below) presents an oligomeric pattern much more similar to hβ2m (Figure 2D). Furthermore, the mβ2m monomer is characterized by a bimodal charge-state distribution (Fig. 2B), suggesting the existence of a minor, at least partially unfolded component, which is not observed in hβ2m. These results indicate a lower conformational stability of the mβ2m variant. To rule out the effects of accidental variability in the experimental conditions, an equimolar mixture of the two β2m variants was analyzed, confirming the presence of the peaks for the unfolded component only for mβ2m (Fig. 2C). Crucially the spectrum of the mixture also revealed that the oligomerization pattern of hβ2m is affected by the presence of mβ2m. β2m heterodimers are formed, but a significant decrease in the amount of hβ2m oligomers is also observed. The ability of mβ2m to interact with hβ2m and to reduce hβ2m oligomerization propensity could be related to the previously reported inhibitory effect of mβ2m on hβ2m aggregation [14, 15].

The crystal structure of monomeric mβ2m reveals localized conformational changes compared to hβ2m

In order to better understand the molecular interactions occurring in the oligomers, the crystal structure of mβ2m was determined to 1.92 Å resolution, providing an electron density of excellent quality (Table 1). As expected, the three-dimensional structure of mβ2m takes a typical β-sandwich fold (Fig. 3A). Interestingly, comparison of the crystal structures of mβ2m and hβ2m reveals that mβ2m resembles more closely to hβ2m or mβ2m when bound to MHC-I [24, 25], compared to soluble monomeric hβ2m [26] (Fig. 3A-C). In particular, the three-dimensional structure of the monomeric mβ2m reveals that the AB loop, connecting the A and B strands, takes the same closed conformation as found in hβ2m when bound to MHC-I (Fig. 3B-C). Furthermore, the D-strand is bulged at residue 53 in both monomeric mβ2m and MHC-I-bound hβ2m compared to monomeric hβ2m (Fig. 3) [17, 21, 27, 28]. This is reflected by the RMSD values of 0.87 Å over 99 Cα and of 1.13 Å over 90 Cα following the superposition of unbound mβ2m onto MHC-I-bound hβ2m or monomeric hβ2m, respectively. Most importantly, several regions considered as highly relevant for hβ2m aggregation present analogous conformational arrangements in monomeric mβ2m. First, Pro32 is in *cis* conformation. This isomerisation from *cis* to *trans* is considered as a fundamental step towards the formation of the aggregation prone intermediate [29]. Furthermore, the aromatic residues (Y10, Y26, F56, W60, F62, Y63), involved in Thioflavin T (ThT) binding [30] and crucial for hβ2m amyloid aggregation [19], display very similar structural conformations in both structures. Finally, a Ramachandran plot analysis of mβ2m reveals that the strained geometry of the DE-loop is perfectly comparable to the one observed in monomeric hβ2m. This loop is directly involved in the destabilisation of the hβ2m fold [23, 31]. In summary, the monomeric structure of mβ2m does not display any major conformational changes in regions known to be relevant for amyloid formation compared to hβ2m.

mβ2m may form DD dimers

To date, several works have proposed that a head to head interaction named DD strand interface, formed between hβ2m molecules, may be the first intermolecular interaction along the β2m aggregation pathway [15, 30, 32, 33]. This DD interface involves several β2m regions, which are all relevant for aggregation including the D-strand as well as the BC and DE loops [32]. Using the crystal structures of monomeric mβ2m and hβ2m, hypothetical molecular models of murine and heterodimeric murine-human DD complexes were created and analysed (Fig. 3D-F). No steric clashes were observed in these molecular models, suggesting that both mβ2m and hβ2m are fully compatible with the formation of a DD interface. Indeed, mixed dimers were also formed (Fig. 2). Moreover, a PISA analysis indicated that the dimer formation between two hβ2m molecules seems to be more energetically favourable compared to the murine dimer (interface area and energy gain on complex formation corresponded 225 Å/-1.1 kcal/mol and 171 Å/-0.2 kcal/mol for dimeric hβ2m and mβ2m, respectively). This result well correlates with the observation that, under native conditions, mβ2m forms significantly less dimers compared to hβ2m (Fig. 2).

mβ2m displays lower stability compared to hβ2m

Since β2m aggregation propensity correlates with thermodynamic stability of the native state [31], the fold stability of the two β2m orthologs was assessed by temperature ramps (temperature slope 50 °C/hour) monitored by Far-UV circular dichroism. Thermal denaturation demonstrated that mβ2m unfolds at lower temperature compared to hβ2m (Tm values of 58.9 ± 0.8 °C and 63.6 ± 1.0 °C for mβ2m and hβ2m, respectively) (Fig. 4A). Unexpectedly, although significantly less amyloidogenic, mβ2m is also less stable than hβ2m.

The structural dynamics of the two protein variants were further investigated by analysis of the reduction kinetics of the internal disulphide bridge formed between the cysteine residues C25 and C80. This process is very slow under non-denaturing conditions for hβ2m, due to the buried structural environment of the disulphide bridge [23, 34]. Monomeric hβ2m and mβ2m were mixed and incubated under native but strongly reducing conditions. Aliquots were collected at different time points and free thiols were alkylated by allyl-bromide. The resulting samples were purified and analyzed by denaturing MS (Fig. 4B). After 30 minutes, both variants remained completely oxidized. The presence of species with reduced/alkylated cysteine residues became evident only after one-hour incubation, when mβ2m became highly reduced (~60%, estimated by the sum of single- and double-alkylated species), while hβ2m remained prevalently in the oxidized form (~80%). After three hours of incubation, approximately 90% and 70% of mβ2m and hβ2m were reduced, respectively. Taken together, these results suggest a higher accessibility of the disulphide bridge within mβ2m compared to hβ2m under these conditions.

mβ2m ensemble does not show high-energy states and displays a lower aggregation propensity

In order to characterise the conformational properties of mβ2m and hβ2m, we first measured and assigned backbone chemical shifts for mβ2m as previously described (Fig. 3G) [35]. Experimental NMR data were already available in the literature for hβ2m [36]. We thereafter employed NMR chemical shifts as restraints in Metadynamics Metainference (M&M) simulations [37]. The resulting M&M simulations were carried out until convergence (Fig. 5) with a statistical error on the resulting conformational free energies of less than 1 kJ/mol. The resulting structural ensembles was then analyzed as a function of the side-chain rotamer distribution (AlphaBeta collective variable; AB) and the antiparallel β-structure content (AntiBetaRMSD CV; anti-β) (Fig. 6A). The resulting free energy surfaces are then comparable with those formerly obtained for other β2m variants [18, 20]. The Free Energy Surface (FES) for hβ2m and mβ2m display remarkable differences. hβ2m is characterized by a global minimum and by the presence of a high-energy low populated state. The global minimum (anti-β variable between 19 and 22, corresponding to a beta content between 38 and 44%) is structurally similar to the crystal structure (average RMSD of 1.5 Å), while the high-energy state (anti-β between 17 and 18 corresponding to a beta content between 34 and 36%) is slightly more disordered (average RMSD of 3 Å). The free energy for mβ2m displays a single minimum with slightly higher average beta content as well as larger fluctuations (anti-β between 19 and 25

corresponding to a beta content between 34 and 36%, and an average RMSD with respect to the crystal of mβ2m of 1.8 Å) compared to hβ2m. Intriguingly, the FES does not reveal the presence of any high-energy state (Fig. 6A). Notably, in a recent work simulations and experiments indicate the presence of a high energy state in both hβ2m and the D76N hβ2m variant characterized by loss of secondary structure [20].

The hβ2m and mβ2m conformational ensembles were subsequently used in combination with the program CamSol to generate a per-residue analysis of the aggregation propensity under native conditions (Fig. 6B). Remarkably, the most relevant difference in the obtained aggregation propensity profiles was observed for residue 85, a valine in hβ2m and an aspartic acid in mβ2m. Interestingly, this position has already been determined as crucial for hβ2m aggregation. Indeed, the rationally designed V85E hβ2m variant displays significantly less aggregation propensity compared to hβ2m with a comparable fold stability [18]. To better distinguish the role of structure and dynamics in determining the aggregation properties of β2m, we also compared the profiles averaged over the ensemble with those calculated from the crystal structures (Fig. 6B). Interestingly, in hβ2m the dynamics increase the surface aggregation propensity, while we observe the opposite behaviour for mβ2m. In fact, the profile calculated over the ensemble for mβ2m displays much less aggregation prone regions compared to the crystal structure.

Thus, the comparison of the M&M conformational ensembles indicates that while the aspartic acid D85 in mβ2m may be critical for its remarkably lower aggregation propensity, the relative dynamics of the two proteins also contribute to either increased (for hβ2m) or decreased (for mβ2m) overall aggregation propensity.

*The presence of V85 increases the aggregation propensity of m*β*2m in vitro*

All previous studies on mβ2m aggregation propensity have focused on the D85 mβ2m variant (herein named mβ2m), but in contrast to hβ2m, several variants of mβ2m have been identified. Among these a valine residue at position 85 has been previously reported [38, 39]. We therefore mutated the aspartate residue at position 85 to a valine and characterized the D85V mβ2m variant (V85 mβ2m) in order to verify the importance of this position in determining mβ2m aggregation propensity. The stability of V85 mβ2m was evaluated by monitoring its thermal denaturation by far-UV CD measurements. Our results revealed that the Tm value for V85 mβ2m is slightly higher compared to mβ2m (61.4 ± 0.8 °C and 58.9 ± 0.8 °C, respectively) (Fig. 7A). Thus, the aspartic acid to valine substitution at position 85 does not alter significantly the overall fold stability of the mutated variant compared to mβ2m. On the other hand, V85 mβ2m has a higher propensity to oligomerize relative to mβ2m, resulting in the formation of a dimeric population similar to the one detected for hβ2m (Fig. 2D). We then assessed the aggregation propensity of V85 mβ2m as described above. Our results demonstrate that, at pH 2.5, V85 mβ2m aggregates considerably compared to mβ2m in the presence of seeds of hβ2m (Fig. 7B). Furthermore, seeds of V85 mβ2m fibrils also successfully triggered hβ2m aggregation but not mβ2m aggregation. Finally, the fibrillar nature of V85 mβ2m aggregates was also verified using transmission electron microscopy (Fig. 7C). Altogether, our results demonstrate that the V85 mutation facilitates mβ2m aggregation, further supporting the key role of this position.

DISCUSSION

β2m has been studied as a model for amyloid aggregation for decades [40]. This protein is of particular interest given that its fold is highly stable, which is a somehow counterintuitive property for an amyloidogenic protein. Indeed, only abnormally high hβ2m concentration over several years triggers aggregation leading to DRA. Interestingly mβ2m is not amyloidogenic *in vivo* or *in vitro* [11] and mixed oligomers of mβ2m with hβ2m seeds inhibit the aggregation capacity of hβ2m [11, 15]. It is well established that mβ2m has a higher saturation concentration compared to hβ2m, resulting in a lower aggregation propensity [13]: However, the results presented within this study suggest in our opinion a more complex picture.

We have previously reported that hβ2m displays a marked tendency to form soluble oligomers under native conditions [23]. Conversely, we here demonstrate that mβ2m displays a very limited tendency to oligomerize, forming relatively small amounts of only dimers. Remarkably, hβ2m oligomerisation is significantly inhibited in presence of mβ2m, even though heterodimers are detectable in mβ2m-hβ2m mixtures. This suggests that the decreased oligomerisation could be mediated by hβ2m-mβ2m protein-protein interactions. (Fig. 2). Moreover, based on the crystal structure of mβ2m, a hypothetical molecular model of a DD-mβ2m dimer was designed, indicating no major structural steric clashes upon dimer formation. Interestingly, the calculated energy gain upon dimer mβ2m formation was significantly reduced compared to hβ2m dimer models, suggesting a less optimized interface in mβ2m dimers compared to hβ2m dimers. This observation may explain several previous results. Karamanos *et al* observed that although the hβ2m/hβ2m homodimer and the mβ2m/hβ2m heterodimer may have comparable interaction interfaces, the formation of the hβ2m/hβ2m homodimer is instrumental to amyloid formation while mβ2m/hβ2m heterodimerization results in an inhibitory complex, impairing amyloid formation [15]. It is thus possible that mβ2m competes with the formation of hβ2m homodimers and either kinetically or thermodynamically impairs the formation of higher order oligomers. Thus altogether, our results suggest that sub-optimal DD interface formed within mβ2m/mβ2m homodimers may protect mβ2m from inducing amyloid aggregation. Similarly, the DD interface formed in mβ2m/hβ2m heterodimers may also perturb the appropriate formation of hβ2m oligomers.

Our results demonstrate that specific segments of mβ2m sequence (residues 60-70 and 80-90), and to a lesser extent the dynamics, play also crucial roles in determining its low aggregation propensity. Indeed, the analyses of the primary sequence and of the computed aggregation propensity of the conformational ensembles indicate that residue D85 plays a key role in the significant reduction of mβ2m aggregation propensity compared to hβ2m. Accordingly, the V85 mβ2m variant presents a oligomerization pattern similar to human wild type and displays an amyloidogenicity comparable to hβ2m under denaturing conditions, while mβ2m is mainly monomeric under non-denaturing conditions, and remains soluble under the same amyloidogenic conditions as previously reported [13]. This is well in line with data showing that residues 83 and 85 are crucial in determining hβ2m aggregation [18].

It thus remains to be determined if the V85 mβ2m variant would display the same amyloidogenicity as hβ2m *in vivo* or if the low oligomerisation tendency observed for mβ2m is sufficient to hinder aggregation. Finally, high-energy, partially misfolded, states have been suggested to play a role in protein aggregation by providing aggregation prone structures [29, 41, 42]. In a recent work on the D76N hβ2m mutant we observed that the aggregation propensity of the high-energy state populated by D76N hβ2m is more pronounced with respect to that of the high-energy state formed by hβ2m and may explain the stronger aggregation propensity of the D76N variant [20]. Consequently, the lack of such state for mβ2m is compatible with the different tendencies of hβ2m and mβ2m to oligomerize and for amyloid fibrils.

The results presented within this study shed additional light on the molecular bases underlying the different aggregation propensities of β2m in human and mouse, and provide new possible mechanisms for mβ2m inhibition of hβ2m aggregation. The possibility of blocking pathologic protein misfolding by using a non-aggregative mβ2m variant may be a tantalizing and generalizable strategy to address amyloid aggregation.

Materials and Methods

Preparation of the human β2m
The hβ2m was expressed and purified as previously reported in [43].

Preparation of the murine β2m

The mβ2m sequence encoding amino acids 1-99 was cloned in a pET-8c plasmid. D to V mutagenesis of mβ2m was performed using the QuikChange Lightning site-directed mutagenesis kit supplied by Agilent (Santa Clara, CA) according to manufacturer instructions. The following primers were used: 5'-GCAGAGTTAAGCATGTCAGTATGGCCGAGCC-3' and 5'-GGCTCGGCCATACTGACATGCTTAACTCTGC-3'.

The expression vectors were transformed into BL21(DE3)pLysS (Novagen). The protein production was IPTG induced and the product was purified as inclusion bodies as for hβ2m. The concentration of the final product was determined spectrophotometrically and purity of the product was assessed by SDS-PAGE under denaturing conditions. Refolding was performed by dialysis at 4 °C against 20 mM Tris HCl pH 7.5. After 24 h, the refolding mixture was concentrated using Amicon concentration devices. Refolded β2m was purified and buffer exchanged into 20 mM Tris HCl pH 7.0 by FPLC using Superdex 75 gel filtration (Pharmacia).

Aggregation assays

Three independent aggregation tests for hβ2m, mβ2m and the V85 mβ2m variant were performed in triplicate using black, clear-bottom, 96-well microplates, the protein concentration of 100 μM was used in all experiments. Plates were incubated in a FLUOstar OPTIMA reader (BMG Labtech, Germany) at 37 °C, over a period of 100 h with intermittent cycles of shaking (1 min, 300 rpm, double-orbital) and rest (30 min). The ThT fluorescence intensity of the aggregates, expressed as arbitrary units (AU), was taken every 30 min using 450 ± 10 nm (excitation) and 480 ± 10 nm (emission) wavelength, with a bottom read and a gain of 1000. All reaction mixes were freshly prepared and optimized for self-assembly or seeding experiments under two different conditions: 50 mM phosphate buffer and 100 mM NaCl, pH 7.4, in the presence of 20% v/v TFE [44]; 50 mM sodium citrate and 100 mM NaCl, pH 2.5 [45].

Transmission electron microscopy analysis

Morphological analysis of V85 mβ2m aggregates were carried out adsorbing 10μL of sample onto carbon-coated 200-mesh grids and staining with UAR replacement (negative staining), using a FEI Tecnai Spirit transmission electron microscope (120 kV) equipped with an Olimpus Soft imaging solutions Megaview camera. Images were taken at 18500 X magnification.

Mass spectrometry

ESI-MS spectra under non-denaturing conditions (50 mM ammonium acetate, pH 7) were acquired by direct injection on a Orbitrap Fusion instrument (ThermoFisher Scientific, Waltham, MA, USA). The main instrumental parameters were: ion-spray voltage, 3.1 kV; source dissociation, 55 V; ion transfer tube temperature, 225 °C; flow rate 2μl/min. Spectra were averaged over 2-minute acquisition.

Disulphide bridge reduction kinetics: mixtures of 25 μM hβ2m and 25 μM mβ2m were incubated at 37 °C in 50 mM ammonium carbonate, 100 mM DTT, pH 8, to reduce disulphide bridges. At different incubation times, 10 μL aliquots were taken and diluted in 90 μL of 20% cold trichloroacetic acid, vortexed and incubated 30 min at 4 °C. Then, the sample was centrifuged at 14000 rpm, 4 °C for 30 min, and the resulting pellet washed with cold acetone. After lyophilization in a Speed Vac system (Analitica De Mori, Milan, IT), the sample was resuspended in 20 μL of 50 mM ammonium carbonate, pH 8, 130 mM allyl bromide and incubated 1 h at room temperature for thiol alkylation. Finally, the sample was buffer-exchanged by C18 ZipTips (Merck Millipore, Burlington, MA, USA), with elution by 50% acetonitrile, 1% formic acid followed by direct injection into the mass spectrometer. Each of the above experiments was repeated at least three times using different protein batches.

Crystallisation and structure determination
Crystallization experiments were performed at 293K using a hanging drop vapour diffusion method with 6 μl of mβ2m (4 mg/ml in 20mM Tris HCl, pH 7.5) mixed with 2 μl of the reservoir solution and equilibrated against 1 ml of the reservoir solution. The best crystals were obtained in 34% PEG 8000 w/v, 100 mM Tris HCl, pH 8.0 and in 40% PEG 6000 w/v, 100 mM Tris HCl, pH 8.0. The crystal was cryo-protected by addition of 34% PEG 400 w/v. Data were collected at BL711 beam line, MAX Laboratory, Lund the 6/9/1999 (λ=1.018Å) and were processed and scaled with DENZO and SCALEPACK [46]. The crystal diffracted up to 1.92Å, it belongs to the space group P2₁2₁2₁ with unit cell dimensions of 36.24 Å, 47.60 Å, 64.94 Å. The data collection statistics are shown in Table 1.
The structure of mß2m was solved by molecular replacement using AMoRe [47], mβ2m from the murine MHC-I complex H-2Dd, (PDB code 1BII) was used as an initial model. One subunits of mβ2m was found in the asymmetric unit, crystals display a 51% solvent content. Refinement was carried with X-PLOR [48] applying strict non-crystallographic symmetry. Last step of refinement was performed in Refmac5 [49]. Statistics for the final model are shown in Table 1.

NMR experiments.
NMR measurements were performed on ^{13}C, ^{15}N labelled mβ2m samples at a concentration of 200 μM. Assignment of the backbone resonances was performed by a combination of ^{1}H-^{15}N HSQC, CBCA(CO)NH, HNCACB, HNCO and HN(CA)CO spectra, collectively providing chemical shifts for ^{13}Cα, ^{13}Cβ, ^{1}HN, ^{13}CO and ^{15}N atoms [35].

NMR was performed at 25°C using a Bruker AVANCE spectrometer operating at proton frequency of 700 MHz, equipped with a triple resonance cryoprobe. NMR data were processed using NMRPipe [50] and analysed using Sparky [51]. Data were processed using the MARS programme [52].

Ensembles determination
The simulations were carried out using GROMACS [53] and PLUMED [54] with the ISDB module [55]. The system was described using the Amber03W force field [56] in explicit TIP4P05 water [57] at 298 K. The starting conformations were taken from the 2YXF and the here reported X-ray structure for the hβ2m and mβ2m, respectively. The structures were protonated and solvated with ~8200 water molecules in a dodecahedron box of ~260 nm³ of volume. The M&M protocol was applied using chemical shifts and a global outlier model for the noise as previously described [37, 58]. Ten replicas of the system were simulated in parallel with a restraint applied on the weighted average value of the back-calculated NMR chemical shifts with a force constant determined on the fly by M&M [59].

All replicas were biased by Parallel Bias Metadynamics [60] along the following four CVs: the antiparallel beta content (the "anti-β" CV), the AlphaBeta CV defined over all the chi-1 angles for the hydrophobic side-chains (the "AB" CV), the AlphaBeta CV defined over all the chi-1 angles for the surface exposed side-chains (the "ABsurf" CV), and the AlphaBeta CV defined over all the phi and psi backbone dihedral angles of the protein (the "bbAB" CV). Definition of the CVs are available in the PLUMED manual. Gaussians deposition was performed with σ values automatically determined by averaging the CV fluctuations over 2000 steps and setting a minimum value of 0.1, 0.12, 0.12, and 0.12, for anti-β, AB, ABsurf, and bbAB, respectively [61]; an initial energy deposition rate of 2.5 kJ/mol/ps and a bias-factor of 20. Furthermore, in order to limit the extent of accessible space along each collective variable and correctly treat the problem of the borders, intervals were set to 12–30, 10–40, 0–33, and 10–42 for the four CVs, respectively. Each replica has been run for a nominal time of 400 ns.

The sampling of the 10 replicas was combined using a simple reweighting scheme based on the final metadynamics bias B where the weight w of a conformation X is given by $w=exp(+B(X)/k_BT)$, with k_B the Boltzmann constant and T the temperature, consistently with the quasi static behaviour at convergence of well-tempered metadynamics [61]. The convergence of the simulations by block analysis, including error estimates, is shown in Fig. 5. All the data and PLUMED input files required to reproduce the results reported in this paper are available on PLUMED-NEST (www.plumed-nest.org), the public repository of the PLUMED consortium as plumID:19.038 [62]. Of notice the free

energy obtained for hβ2m resembles that previously determined by replica-averaged metadynamics simulations on a slightly different sequence [18, 63]. The main differences being the lack of a more 'crystal'-like high-energy state and the presence of a slightly more disordered, high-energy, state. This latter was not sampled in a former work [18] because the sampling was not allowed in that region, but was more recently observed by solid state NMR and replica-averaged metadynamics simulations [20].

Circular dichroism

Thermal stability experiments were performed in triplicate using three independent batches of protein and were monitored in the far-UV region using a J-810 spectropolarimeter (JASCO Corp., Tokyo, Japan) equipped with a Peltier system for temperature control. The protein concentration was 0.1 mg/mL in 50 mM sodium phosphate pH 7.4. The temperature ramps were carried out from 20 to 95 °C (temperature slope 50 °C/hour) in a 0.1 cm path length cuvette and monitored at 202 nm wavelength. Tm was calculated as the first-derivative minimum of the traces. Spectra before and after unfolding ramp were recorded (260–190 nm). All three β2m variants considered in this work display an irreversible unfolding under the tested conditions.

Accession number

Atomic coordinates and structure factors for mβ2m have been deposited at the Protein Data Bank, with accession code 6I8C.

REFERENCES

1. Bjorkman, P. J., Saper, M. A., Samraoui, B., Bennett, W. S., Strominger, J. L. & Wiley, D. C. (1987) Structure of the human class I histocompatibility antigen, HLA-A2, *Nature.* **329**, 506-12.

2. Hafstrand, I., Doorduijn, E. M., Duru, A. D., Buratto, J., Oliveira, C. C., Sandalova, T., van Hall, T. & Achour, A. (2016) The MHC Class I Cancer-Associated Neoepitope Trh4 Linked with Impaired Peptide Processing Induces a Unique Noncanonical TCR Conformer, *J Immunol.* **196**, 2327-34.

3. Madhurantakam, C., Duru, A. D., Sandalova, T., Webb, J. R. & Achour, A. (2012) Inflammation-associated nitrotyrosination affects TCR recognition through reduced stability and alteration of the molecular surface of the MHC complex, *Plos One.* **7**, e32805.

4. Uchtenhagen, H., Abualrous, E. T., Stahl, E., Allerbring, E. B., Sluijter, M., Zacharias, M., Sandalova, T., van Hall, T., Springer, S., Nygren, P. A. & Achour, A. (2013) Proline substitution independently enhances H-2D(b) complex stabilization and TCR recognition of melanoma-associated peptides, *European journal of immunology.* **43**, 3051-60.

5. van Stipdonk, M. J., Badia-Martinez, D., Sluijter, M., Offringa, R., van Hall, T. & Achour, A. (2009) Design of agonistic altered peptides for the robust induction of CTL directed towards H-2Db in complex with the melanoma-associated epitope gp100, *Cancer research.* **69**, 7784-92.

6. Halabelian, L., Ricagno, S., Giorgetti, S., Santambrogio, C., Barbiroli, A., Pellegrino, S., Achour, A., Grandori, R., Marchese, L., Raimondi, S., Mangione, P. P., Esposito, G., Al-Shawi, R., Simons, J. P., Speck, I., Stoppini, M., Bolognesi, M. & Bellotti, V. (2014) Class I Major Histocompatibility Complex, the Trojan Horse for Secretion of Amyloidogenic beta2-Microglobulin, *The Journal of biological chemistry.* **289**, 3318-27.

7. Floege, J. & Ehlerding, G. (1996) Beta-2-microglobulin-associated amyloidosis, *Nephron.* **72**, 9-26.

8. Valleix, S., Gillmore, J. D., Bridoux, F., Mangione, P. P., Dogan, A., Nedelec, B., Boimard, M., Touchard, G., Goujon, J. M., Lacombe, C., Lozeron, P., Adams, D., Lacroix, C.,

Maisonobe, T., Plante-Bordeneuve, V., Vrana, J. A., Theis, J. D., Giorgetti, S., Porcari, R., Ricagno, S., Bolognesi, M., Stoppini, M., Delpech, M., Pepys, M. B., Hawkins, P. N. & Bellotti, V. (2012) Hereditary systemic amyloidosis due to Asp76Asn variant beta2-microglobulin, *N Engl J Med.* **366**, 2276-83.

9. Gejyo, F., Yamada, T., Odani, S., Nakagawa, Y., Arakawa, M., Kunitomo, T., Kataoka, H., Suzuki, M., Hirasawa, Y., Shirahama, T., Cohen, A. S. & Schimd, K. (1985) A new form of amyloid protein associated with chronic hemodialysis was identified as beta 2-microglobulin, *Biochemical and biophysical research communications.* **129**, 701-6.

10. Niwa, T. (1997) Beta2-Microglobulin dialysis amyloid and its formation: role of 3-deoxyglucosone and advanced glycation end products, *Nephron.* **76**, 373-91.

11. Ivanova, M. I., Sawaya, M. R., Gingery, M., Attinger, A. & Eisenberg, D. (2004) An amyloid-forming segment of beta2-microglobulin suggests a molecular model for the fibril, *Proceedings of the National Academy of Sciences of the United States of America.* **101**, 10584-9.

12. Zhang, P., Fu, X., Sawashita, J., Yao, J., Zhang, B., Qian, J., Tomozawa, H., Mori, M., Ando, Y., Naiki, H. & Higuchi, K. (2010) Mouse model to study human A beta2M amyloidosis: generation of a transgenic mouse with excessive expression of human beta2-microglobulin, *Amyloid : the international journal of experimental and clinical investigation : the official journal of the International Society of Amyloidosis.* **17**, 50-62.

13. Pashley, C. L., Hewitt, E. W. & Radford, S. E. (2016) Comparison of the aggregation of homologous beta2-microglobulin variants reveals protein solubility as a key determinant of amyloid formation, *Journal of molecular biology.* **428**, 631-643.

14. Eichner, T., Kalverda, A. P., Thompson, G. S., Homans, S. W. & Radford, S. E. (2011) Conformational conversion during amyloid formation at atomic resolution, *Molecular cell.* **41**, 161-72.

15. Karamanos, T. K., Kalverda, A. P., Thompson, G. S. & Radford, S. E. (2014) Visualization of transient protein-protein interactions that promote or inhibit amyloid assembly, *Molecular cell.* **55**, 214-26.

16. de Rosa, M., Barbiroli, A., Giorgetti, S., Mangione, P. P., Bolognesi, M. & Ricagno, S. (2015) Decoding the Structural Bases of D76N ss2-Microglobulin High Amyloidogenicity through Crystallography and Asn-Scan Mutagenesis, *Plos One.* **10**, e0144061.

17. Ricagno, S., Raimondi, S., Giorgetti, S., Bellotti, V. & Bolognesi, M. (2009) Human beta-2 microglobulin W60V mutant structure: Implications for stability and amyloid aggregation, *Biochemical and biophysical research communications.* **380**, 543-7.

18. Camilloni, C., Sala, B. M., Sormanni, P., Porcari, R., Corazza, A., De Rosa, M., Zanini, S., Barbiroli, A., Esposito, G., Bolognesi, M., Bellotti, V., Vendruscolo, M. & Ricagno, S. (2016) Rational design of mutations that change the aggregation rate of a protein while maintaining its native structure and stability, *Scientific reports.* **6**, 25559.

19. Platt, G. W., Routledge, K. E., Homans, S. W. & Radford, S. E. (2008) Fibril growth kinetics reveal a region of beta2-microglobulin important for nucleation and elongation of aggregation, *Journal of molecular biology.* **378**, 251-63.

20. Le Marchand, T., de Rosa, M., Salvi, N., Sala, B. M., Andreas, L. B., Barbet-Massin, E., Sormanni, P., Barbiroli, A., Porcari, R., Sousa Mota, C., de Sanctis, D., Bolognesi, M., Emsley, L., Bellotti, V., Blackledge, M., Camilloni, C., Pintacuda, G. & Ricagno, S. (2018) Conformational dynamics in crystals reveal the molecular bases for D76N beta-2 microglobulin aggregation propensity, *Nature communications.* **9**, 1658.

21. Esposito, G., Ricagno, S., Corazza, A., Rennella, E., Gumral, D., Mimmi, M. C., Betto, E., Pucillo, C. E., Fogolari, F., Viglino, P., Raimondi, S., Giorgetti, S., Bolognesi, B., Merlini, G.,

Stoppini, M., Bolognesi, M. & Bellotti, V. (2008) The controlling roles of Trp60 and Trp95 in beta2-microglobulin function, folding and amyloid aggregation properties, *Journal of molecular biology.* **378**, 885-95.

22. Sormanni, P., Aprile, F. A. & Vendruscolo, M. (2015) The CamSol method of rational design of protein mutants with enhanced solubility, *Journal of molecular biology.* **427**, 478-90.

23. Santambrogio, C., Ricagno, S., Colombo, M., Barbiroli, A., Bonomi, F., Bellotti, V., Bolognesi, M. & Grandori, R. (2010) DE-loop mutations affect beta2 microglobulin stability, oligomerization, and the low-pH unfolded form, *Protein Sci.* **19**, 1386-94.

24. Achour, A., Harris, R. A., Persson, K., Sundback, J., Sentman, C. L., Schneider, G., Lindqvist, Y. & Karre, K. (1999) Murine class I major histocompatibility complex H-2Dd: expression, refolding and crystallization, *Acta crystallographica.* **55**, 260-2.

25. Achour, A., Michaelsson, J., Harris, R. A., Ljunggren, H. G., Karre, K., Schneider, G. & Sandalova, T. (2006) Structural basis of the differential stability and receptor specificity of H-2Db in complex with murine versus human beta2-microglobulin, *Journal of molecular biology.* **356**, 382-96.

26. Iwata, K., Fujiwara, T., Matsuki, Y., Akutsu, H., Takahashi, S., Naiki, H. & Goto, Y. (2006) 3D structure of amyloid protofilaments of beta2-microglobulin fragment probed by solid-state NMR, *Proceedings of the National Academy of Sciences of the United States of America.* **103**, 18119-24.

27. Iwata, K., Matsuura, T., Sakurai, K., Nakagawa, A. & Goto, Y. (2007) High-resolution crystal structure of beta2-microglobulin formed at pH 7.0, *Journal of biochemistry.* **142**, 413-9.

28. Ricagno, S., Colombo, M., de Rosa, M., Sangiovanni, E., Giorgetti, S., Raimondi, S., Bellotti, V. & Bolognesi, M. (2008) DE loop mutations affect beta-2 microglobulin stability and amyloid aggregation, *Biochemical and biophysical research communications.* **377**, 146-50.

29. Chiti, F., De Lorenzi, E., Grossi, S., Mangione, P., Giorgetti, S., Caccialanza, G., Dobson, C. M., Merlini, G., Ramponi, G. & Bellotti, V. (2001) A partially structured species of beta 2-microglobulin is significantly populated under physiological conditions and involved in fibrillogenesis, *The Journal of biological chemistry.* **276**, 46714-21.

30. Halabelian, L., Relini, A., Barbiroli, A., Penco, A., Bolognesi, M. & Ricagno, S. (2015) A covalent homodimer probing early oligomers along amyloid aggregation, *Scientific reports.* **5**, 14651.

31. Ami, D., Ricagno, S., Bolognesi, M., Bellotti, V., Doglia, S. M. & Natalello, A. (2012) Structure, stability, and aggregation of beta-2 microglobulin mutants: insights from a Fourier transform infrared study in solution and in the crystalline state, *Biophys J.* **102**, 1676-84.

32. Colombo, M., de Rosa, M., Bellotti, V., Ricagno, S. & Bolognesi, M. (2012) A recurrent D-strand association interface is observed in beta-2 microglobulin oligomers, *FEBS J.* **279**, 1131-43.

33. Rennella, E., Cutuil, T., Schanda, P., Ayala, I., Gabel, F., Forge, V., Corazza, A., Esposito, G. & Brutscher, B. (2013) Oligomeric states along the folding pathways of beta2-microglobulin: kinetics, thermodynamics, and structure, *Journal of molecular biology.* **425**, 2722-36.

34. Hong, D. P., Gozu, M., Hasegawa, K., Naiki, H. & Goto, Y. (2002) Conformation of beta 2-microglobulin amyloid fibrils analyzed by reduction of the disulfide bond, *The Journal of biological chemistry.* **277**, 21554-60.

35. Patel, J. R., Xu, Y., Capitini, C., Chiti, F. & De Simone, A. (2018) Backbone NMR assignments of HypF-N under conditions generating toxic and non-toxic oligomers, *Biomolecular NMR assignments.* **12**, 273-277.

36. Beerbaum, M., Ballaschk, M., Erdmann, N., Schnick, C., Diehl, A., Uchanska-Ziegler, B., Ziegler, A. & Schmieder, P. (2013) NMR spectroscopy reveals unexpected structural variation at the protein-protein interface in MHC class I molecules, *Journal of biomolecular NMR.* **57**, 167-78.

37. Bonomi, M., Camilloni, C. & Vendruscolo, M. (2016) Metadynamic metainference: Enhanced sampling of the metainference ensemble using metadynamics, *Scientific reports.* **6**, 31232.

38. Gates, F. T., 3rd, Coligan, J. E. & Kindt, T. J. (1981) Complete amino acid sequence of murine beta 2-microglobulin: structural evidence for strain-related polymorphism, *Proceedings of the National Academy of Sciences of the United States of America.* **78**, 554-8.

39. Hermel, E., Robinson, P. J., She, J. X. & Lindahl, K. F. (1993) Sequence divergence of B2m alleles of wild Mus musculus and Mus spretus implies positive selection, *Immunogenetics.* **38**, 106-16.

40. Merlini, G. & Bellotti, V. (2003) Molecular mechanisms of amyloidosis, *N Engl J Med.* **349**, 583-96.

41. Chiti, F., Mangione, P., Andreola, A., Giorgetti, S., Stefani, M., Dobson, C. M., Bellotti, V. & Taddei, N. (2001) Detection of two partially structured species in the folding process of the amyloidogenic protein beta 2-microglobulin, *Journal of molecular biology.* **307**, 379-91.

42. Neudecker, P., Robustelli, P., Cavalli, A., Walsh, P., Lundstrom, P., Zarrine-Afsar, A., Sharpe, S., Vendruscolo, M. & Kay, L. E. (2012) Structure of an intermediate state in protein folding and aggregation, *Science (New York, NY.* **336**, 362-6.

43. Esposito, G., Michelutti, R., Verdone, G., Viglino, P., Hernandez, H., Robinson, C. V., Amoresano, A., Dal Piaz, F., Monti, M., Pucci, P., Mangione, P., Stoppini, M., Merlini, G., Ferri, G. & Bellotti, V. (2000) Removal of the N-terminal hexapeptide from human beta2-microglobulin facilitates protein aggregation and fibril formation, *Protein Sci.* **9**, 831-45.

44. Yamamoto, S., Yamaguchi, I., Hasegawa, K., Tsutsumi, S., Goto, Y., Gejyo, F. & Naiki, H. (2004) Glycosaminoglycans enhance the trifluoroethanol-induced extension of beta 2-microglobulin-related amyloid fibrils at a neutral pH, *J Am Soc Nephrol.* **15**, 126-33.

45. Naiki, H., Haschimoto, N., Suzuki, S., Rimura, H., Nakakuki, K. & Gejyo, F. (1997) Establishment of a kinetic model of dialysis-related amyloid fibril extension in vitro., *AMYLOID: Int Exp Clin Invest.* **4**, 223-32.

46. Otwinowski, Z. (1993) Oscillation Data Reduction Program, Daresbury Laboratory, Warrington, United Kingdom.

47. Navaza, J. (2001) Implementation of molecular replacement in AMoRe, *Acta crystallographica.* **57**, 1367-72.

48. Brunger, A. T., Adams, P. D., Clore, G. M., DeLano, W. L., Gros, P., Grosse-Kunstleve, R. W., Jiang, J. S., Kuszewski, J., Nilges, M., Pannu, N. S., Read, R. J., Rice, L. M., Simonson, T. & Warren, G. L. (1998) Crystallography & NMR system: A new software suite for macromolecular structure determination, *Acta crystallographica.* **54**, 905-21.

49. Murshudov, G. N., Vagin, A. A. & Dodson, E. J. (1997) Refinement of macromolecular structures by the maximum-likelihood method, *Acta crystallographica.* **53**, 240-55.

50. Delaglio, F., Grzesiek, S., Vuister, G. W., Zhu, G., Pfeifer, J. & Bax, A. (1995) NMRPipe: a multidimensional spectral processing system based on UNIX pipes, *Journal of biomolecular NMR.* **6**, 277-93.

51. Lee, W., Tonelli, M. & Markley, J. L. (2015) NMRFAM-SPARKY: enhanced software for biomolecular NMR spectroscopy, *Bioinformatics.* **31**, 1325-7.

52. Jung, Y. S. & Zweckstetter, M. (2004) Mars -- robust automatic backbone assignment of proteins, *Journal of biomolecular NMR.* **30**, 11-23.

53. Abraham, M. J., Murtola, T., Schulz, R., Pall, S., Smith, J. C., Hess, B. & Lindhal, E. (2015) GROMACS: High performance molecular simulations through multi-level parallelism from laptops to supercomputers. , *SoftwareX.* **1-2**, 19-25.

54. Tribello, G. A., Bonomi, F., Branduardi, D., Camilloni, C. & Bussi, G. (2014) PLUMED 2: New feathers for an old bird, *Computer Physics Communications.* **182**, 604-13.

55. Bonomi, M. & Camilloni, C. (2017) Integrative structural and dynamical biology with PLUMED-ISDB, *Bioinformatics.* **33**, 3999-4000.

56. Best, R. B. & Mittal, J. (2010) Protein simulations with an optimized water model: cooperative helix formation and temperature-induced unfolded state collapse, *The journal of physical chemistry B.* **114**, 14916-23.

57. Abascal, J. L. & Vega, C. (2005) A general purpose model for the condensed phases of water: TIP4P/2005, *The Journal of chemical physics.* **123**, 234505.

58. Bonomi, M., Camilloni, C., Cavalli, A. & Vendruscolo, M. (2016) Metainference: A Bayesian inference method for heterogeneous systems, *Science advances.* **2**, e1501177.

59. Lohr, T., Jussupow, A. & Camilloni, C. (2017) Metadynamic metainference: Convergence towards force field independent structural ensembles of a disordered peptide, *The Journal of chemical physics.* **146**, 165102.

60. Pfaendtner, J. & Bonomi, M. (2015) Efficient Sampling of High-Dimensional Free-Energy Landscapes with Parallel Bias Metadynamics, *Journal of chemical theory and computation.* **11**, 5062-7.

61. Branduardi, D., Bussi, G. & Parrinello, M. (2012) Metadynamics with Adaptive Gaussians, *Journal of chemical theory and computation.* **8**, 2247-54.

62. Consortium, T. P. (2019) The PLUMED consortium: A community effort to promote openness, transparency and reproducibility in molecular simulations, *Submitted*.

63. Camilloni, C. & Vendruscolo, M. (2014) Statistical mechanics of the denatured state of a protein using replica-averaged metadynamics, *Journal of the American Chemical Society.* **136**, 8982-91.

Table 1. Data collection and refinement statistics for the structure of mβ2m

PDB code	6I8C
Space group	$P2_12_12_1$
Cell a,b,c (Å)	36.24 47.60 64.94
Resolution (Å)	38-1.92 (1.95-1.92)
Number of unique reflections	8882 (572)
Completeness (%)	98.6 (96.8)
Redundancy	4.4 (4.3)
I/σ	20.1 (7.3)
Rsym (%)	4.4 (13.2)

Refinement statistics

Resolution (Å)	28.85-1.92
R work (%)	18.32
R free (%)	22.20

Number of atoms

All	934
Protein	842
Water	87
Ligand	5

Mean isotropic B-factor ($Å^2$)

Protein main-chain atoms	20.46
Protein side chain atoms	24.20
Water	32.10

Rmsd from ideal values

Bond length (Å)	0.007
Bond angles (°)	1.152

Ramachandran plot statistics

Residues in preferred regions (%)	98.97
Residues in allowed regions (%)	1.03
Outliers (%)	0

Author Contributions: A.A., L.B., X.H., R.S., C.S., J.B., C.V., A.B., C.M.G.D.L., P.S., F.M., A.D.S., T.S., and C.C. performed the experiments; A.A., R.G., C.C. and S.R. designed the study; A.A., R.G., C.C. and S.R. wrote the paper with contributions from all other authors.

Conflict of interest: The authors declare that they have no conflicts of interest with the contents of this article.
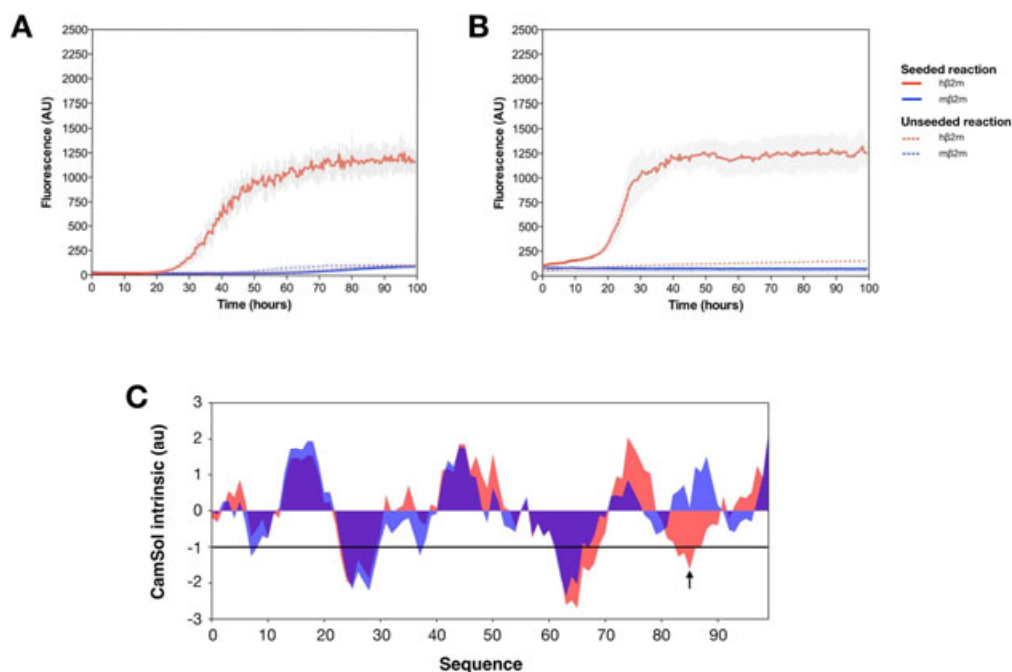
Figure 1. (A, B) The kinetics of fibril formation were monitored by fluorescence using the ThT binding assay. Monomeric mβ2m (blue) and hβ2m (red) were incubated at 37 °C under two different aggregation conditions at pH 7.4 (A) and at pH 2.5 (B).

(C) CamSol intrinsic solubility scores of hβ2m (red) and mβ2m (blue). A score greater than 1 indicates highly soluble sites while a score lower than −1 indicates aggregation-prone sites. The two profiles reveal that in contrast to mβ2m, the regions corresponding to residues 60-70 and 80-90 in hβ2m are prone to aggregation. The black arrow indicates the position of residue 85.
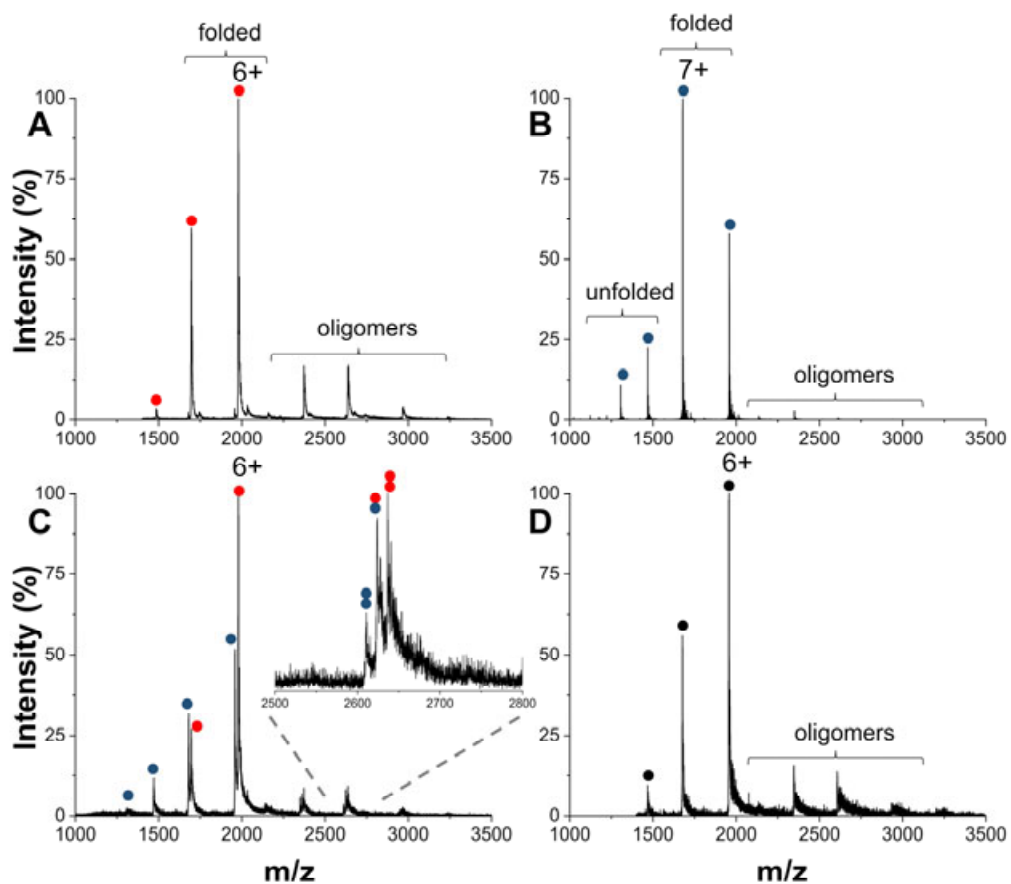
Figure 2. (A) ESI-MS spectra of 75 µM hβ2m; (B) 75 µM mβ2m; (C) a mix of 75 µM hβ2m and 75 µM mβ2m; (D) 75 µM V85 mβ2m. The most intense peak in each panel is labeled by the corresponding charge state. In (A), (B) and (D), the peaks corresponding to distinct species are grouped by braces. The inset of panel C is a magnification of the 9+ signals of the dimer. Red, blue and black circles correspond to the subunits of hβ2m, mβ2m and V85 mβ2m, respectively.
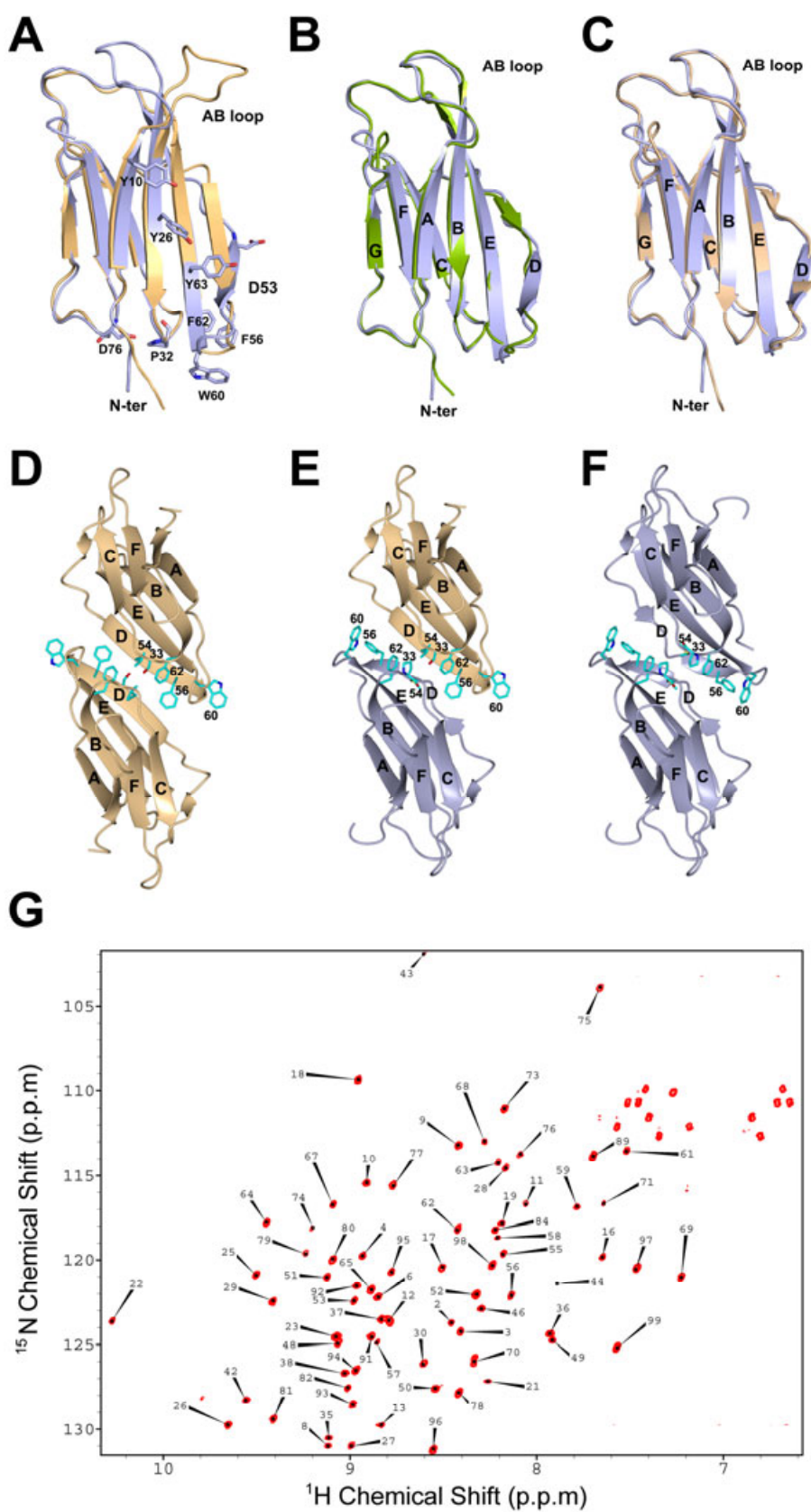
Figure 3. (A-C) Comparisons of the crystal structures of the mβ2m in purple with A) the structure of monomeric hβ2m in orange (pdb code: 1LDS); B) the structure of mβ2m from an MHC I complex in green (pdb code: 1BII); C) the structure of hβ2m from a complex with mouse MHC I, H-2Dd in beige (pdb code 2F74). (D-F) Models of DD dimers built using the structures of D) two monomeric hβ2m; E) one mβ2m and hβ2m; F) two monomeric mβ2m. Main residues involved in the interface as reported in [32] are shown. These models suggest that mβ2m and hβ2m structures are compatible with the formation of homo and hetero DD dimers. (G) NMR HSQC spectrum of mβ2m at 25"C, peaks are well resolved and 78 out 100 can be uniquely assigned.
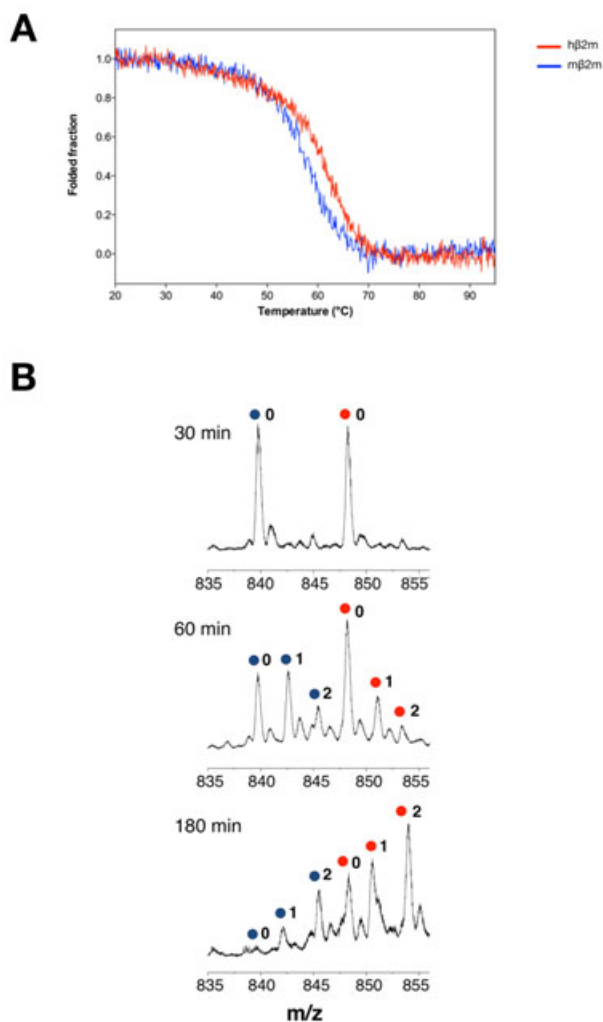
Figure 4. (A) Thermal unfolding of 8.5 µM mβ2m and hβ2m in 50 mM sodium phosphate pH 7.4 monitored by far-UV CD at 202 nm. (B) Kinetics of disulphide bridge reduction. Magnification of the 14+ peaks of nano-ESI-MS spectra obtained from equimolar (25 µM) mixtures of hβ2m (red circle) and mβ2m (blue circle), incubated in 100 mM DTT for 30, 60 or 180 min, and alkylated by allyl bromide. Peaks are labeled according to the number of the incorporated propyl groups.
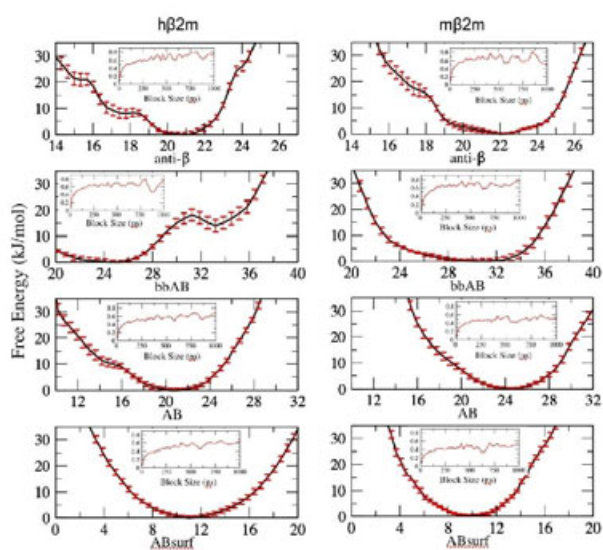
Figure 5. Free energy profiles and error estimates (inset) in kJ/mol for the hβ2m (left) and the mβ2m ensembles, respectively. The free energy profiles are plotted as a function of the four biased collective variables (see Materials and Methods). The corresponding error estimates are obtained by block analysis and plotted as a function of the block size, that is the extent in ns of the time window employed for the calculation (see Materials and Methods).
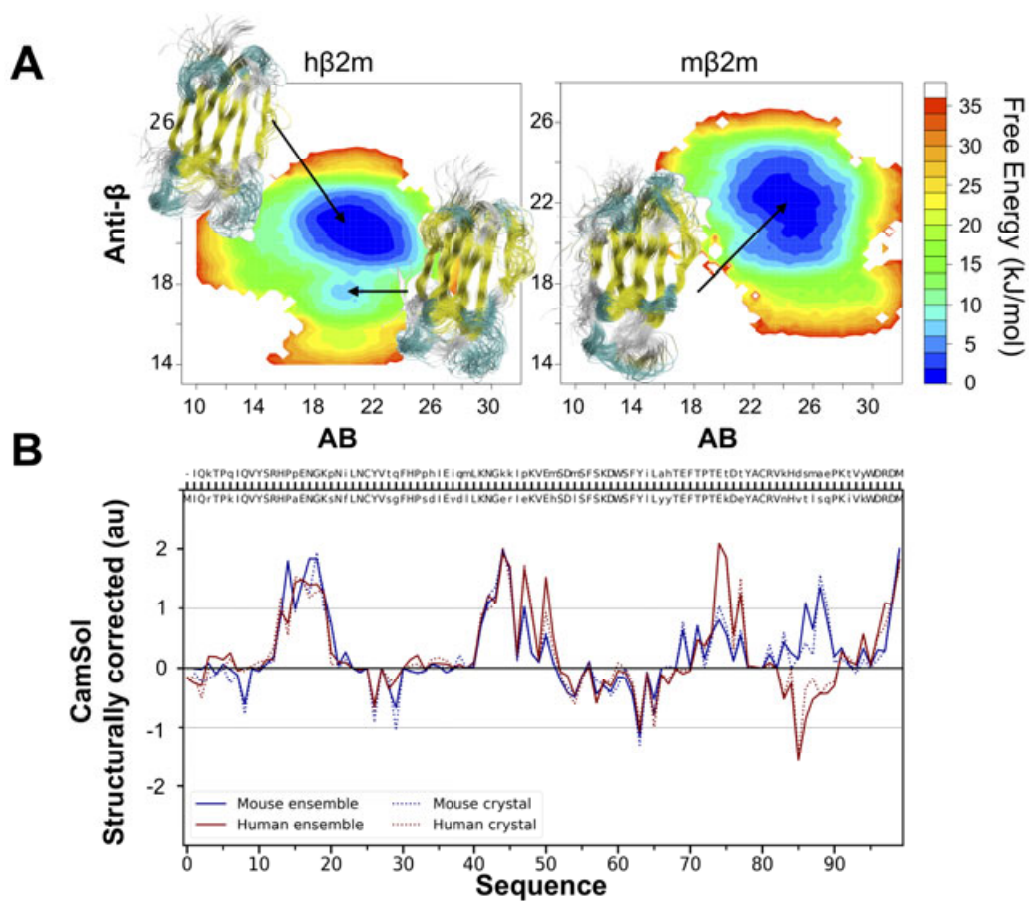
Figure 6. (A, B) Free energy surfaces for hβ2m and mβ2m, respectively. The surfaces are shown as a function of the side chain rotameric state, AB, and the antiparallel β-structure content (anti-β). (C) CamSol structurally corrected solubility scores for the hβ2m (red solid) and mβ2m (blue solid) conformational ensembles as well as for the hβ2m and mβ2m crystal structures (red dotted and blue dotted, respectively). A score greater than 1 indicates a highly soluble site while a score lower than −1 indicates an aggregation-prone site.
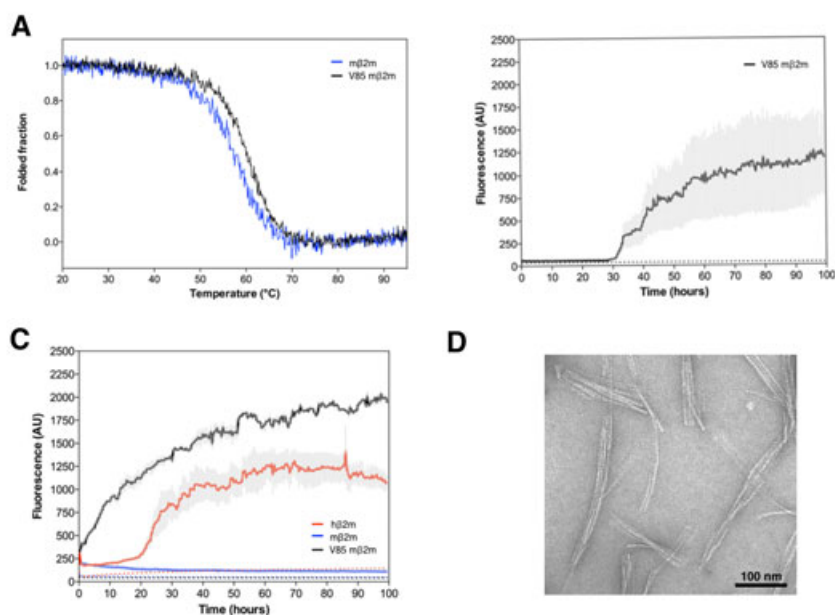
Figure 7. (A) Thermal unfolding of 8.5 µM mβ2m and V85 mβ2m in 50 mM sodium phosphate pH 7.4 monitored by far-UV CD at 202 nm. (B, C) Kinetics of fibril formation monitored by fluorescence in the ThT binding assay. The V85 mβ2m was incubated at pH 2.5 in the presence of preformed hβ2m seeds (B); hβ2m, mβ2m and V85 mβ2m were incubated in the presence of preformed V85 mβ2m seeds at pH 2.5. Seeded and unseeded reactions are shown in solid and dashed lines, respectively. (D) Transmission electron microscopy micrograph shows fibrillar aggregates of the V85 mβ2m variant.